A thermodynamic study of the influence of the Al2O3 content on the CaO-SiO2-YO1.5 system

J. Bonnal, S. Mermoul, C. Petitjean, P.J. Panteix, D. Bonina, C. Gendarme, S. Arnal, M. Vilasi

A thermodynamic study of the influence of the Al_2O_3 content on the $CaO\text{-}SiO_2\text{-}YO_{1.5}$ system

J. Bonnal[1], S. Mermoul[1], C. Petitjean[1], P.J. Panteix[1*], D. Bonina[1], C. Gendarme[1], S. Arnal[2], M. Vilasi[1]

[1]Université de Lorraine, CNRS, IJL, F-54000 Nancy, France

[2]Safran Ceramics, 33700 Mérignac, France

[*]Corresponding author : pierre-jean.panteix@univ-lorraine.fr

Abstract

In aircraft engines applications, the interactions between rare earth silicates (mainly yttrium silicates) used as Environmental Barrier Coatings (EBCs) on turbine blades and liquid calcium-magnesium-aluminosilicates (CMAS) due to the particles ingested by the engines may lead to severe damages at high temperature. Due to the large range of composition of CMAS, simplified model systems must be used to have a good comprehension of the thermochemical phenomena leading to degradation. The interaction between ceramics and CMAS can lead to the precipitation of phases as apatite $Ca_2Y_8(SiO_4)_6O_2$ and cyclosilicate $Ca_3Y_2(Si_3O_9)_2$ which might provide protection to the EBC. However, their thermodynamic stability depends on many parameters. In the present work, the influence of alumina Al_2O_3 addition to the ternary system $CaO\text{-}SiO_2\text{-}YO_{1.5}$ has been studied in order to verify the equilibrium with the liquid field at 1300°C.

Keywords

CMAS, Environmental Barrier Coating (EBC), Yttrium silicates, Thermochemistry, Equilibrium

1. Introduction

The amelioration of the performances of aircraft engines requires an increase of the working temperature. New turbine blade materials have been developed in order to withstand high

temperature ranges, as ceramic matrix composites (i.e. CMCs) [1]. The degradation of these ceramics by combustion products can significantly limit their lifetime, and their protection by Environmental Barrier Coatings (EBCs) is thus required. In this application, rare-earth (RE) silicates, such as rare earth disilicates $RE_2Si_2O_7$, are considered as good candidates [2]. However, the development of EBCs is hindered by the high-temperature corrosion due to interactions with liquid calcium-magnesium-aluminosilicates (CMAS) [3-5]. Indeed, the infiltration of these silicate melts into the coating causes thermochemical degradations by acido-basic dissolution of the RE-silicate in the melt and the precipitation of new phases [6,7].

Many parameters, as the temperature, the composition of the melt (i.e. basicity, viscosity), or the nature of the EBC, can modify the kinetics and equilibrium between RE-silicate and CMAS [8]. Consequently, the consideration of thermodynamic aspects is of prime importance to reach a full comprehension of the mechanisms of the corrosion of EBC by CMAS. These systems are quite complex, and a simplification of the compositions is thus required to determine all the mechanisms. The CMAS composition can be limited to a three oxides system containing only calcia, alumina and silica (CAS). The interaction with a rare-earth disilicate $RE_2Si_2O_7$ thus leads to consider a CaO-$AlO_{1.5}$-SiO_2-$REO_{1.5}$ quaternary system. However, previous works have described the phases at equilibrium in ternary systems such as CaO-SiO_2-$YO_{1.5}$ [9] or CaO-SiO_2-$GdO_{1.5}$ [10] at 1400°C and 1600°C. These phase diagrams do not take into account the presence of alumina Al_2O_3, and only one liquid phase is reported in these works. However, a large range of composition is reported in the literature for CMAS, i.e. molten silicates [11-14]. The extent of the liquid field in a RE_2O_3-CaO-SiO_2 in presence of alumina, magnesia and iron oxide has also already been proven [15].

The purpose of the present study is to focus on the influence of alumina Al_2O_3 in the CaO-SiO_2-$YO_{1.5}$ system at 1300°C. Attention will be paid on the modification of equilibrium state (nature and composition of the precipitated phases), on the liquid composition (including the solubility of yttrium), and more specifically on the extent of the liquid field at 1300°C. One purpose is to investigate the existence of an equilibrium between apatite and liquid in this temperature range, which has not been reported yet in these systems. The phase diagram of the CaO-SiO_2-$YO_{1.5}$ system reported by Poerschke et al. at 1400°C in Figure 1 shows the small extent of the liquid field in this simplified system. Two types of starting mixes are chosen, close to this liquid field, in areas with different equilibria. The purpose is to observe the influence of alumina addition on both extent of liquid field and nature of the precipitated phases at equilibrium. The first mix is silica-rich and composed of 22 mol% CaO, 70 mol.% SiO_2 and 8 mol%$YO_{1.5}$ (blue square

on Figure 1): it is noted as $C_{22}S_{70}Y_8$. It is located in the area where silica SiO_2 and cyclosilicate $Ca_3Y_2(Si_3O_9)_2$ are in equilibrium with the liquid. The second mix is silica-poor and composed of 30 mol.% CaO, 50 mol.% SiO_2 and 20 mol.% $YO_{1.5}$. (red circle on Figure 1): it is noted as $C_{30}S_{50}Y_{20}$. It is located in the area where pseudo-wollastonite $CaSiO_3$ is in equilibrium with cyclosilicate and apatite.

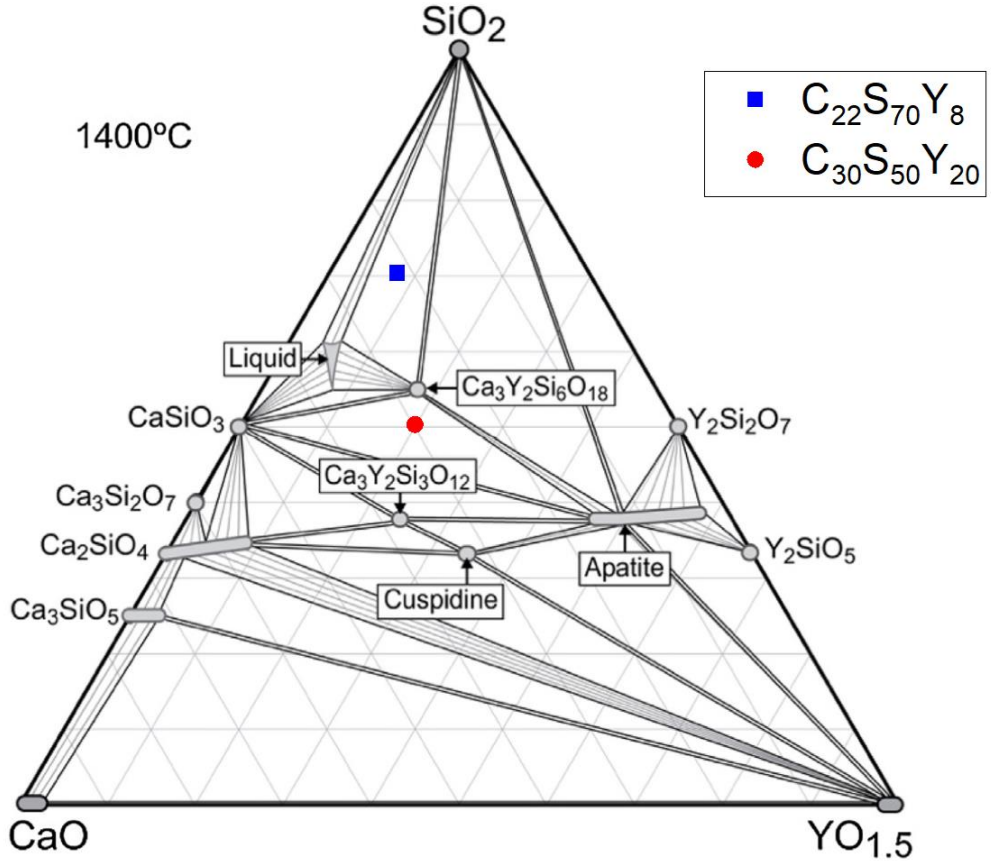

Figure 1. Compositions of the two systems $C_{22}S_{70}Y_8$ and $C_{30}S_{50}Y_{20}$ chosen for this work represented on the isotherm section à 1400°C of the CaO-SiO_2-$YO_{1.5}$ phase diagram proposed by Poerschke et al. [9]

2. Materials and methods

2.1. Mixes preparation

Both compositions $C_{22}S_{70}Y_8$ and $C_{30}S_{50}Y_{20}$ were respectively added with 2, 5, 8, 9 and 10 mol.% of Al_2O_3. The theoretical compositions of the quaternary mixes are reported in Table 1. The samples were prepared by mixing the following precursors: $CaCO_3$ (99.0%, Alfa Aesar), Al_2O_3 (99.0%, Alfa Aesar), amorphous SiO_2 (99.8%, Alfa Aesar) and Y_2O_3 (99.9., Alfa Aesar). Mixes of 2 g of each composition were homogenized in dry conditions at 2500 rpm during 15 minutes

by using a planetary ball mill (Fritsch Pulverisette 7), with a zirconia grinding bowl (volume = 12 mL) and three zirconia balls (diameter = 10 mm). The precursors mixtures were then heat treated in air in $Pt_{95}Au_5$ crucibles at 1300°C during 260 h, this duration being chosen in order to ensure the attainment of thermodynamic equilibrium.

Table 1. Theoretical composition (mol.%) of $C_{22}S_{70}Y_8$ and $C_{30}S_{50}Y_{20}$ mixes after addition of Al_2O_3 (mol.%)

$C_{22}S_{70}Y_8$	**CaO**	**SiO_2**	**Y_2O_3**	**Al_2O_3**
0%Al_2O_3	22.9	72.9	4.2	0.0
2%Al_2O_3	22.4	71.5	4.1	2.0
5%Al_2O_3	21.8	69.4	4.0	4.8
8%Al_2O_3	21.2	67.5	3.9	7.4
9%Al_2O_3	21.0	66.9	3.8	8.3
10%Al_2O_3	20.8	66.3	3.8	9.1
$C_{30}S_{50}Y_{20}$	**CaO**	**SiO_2**	**Y_2O_3**	**Al_2O_3**
0%Al_2O_3	33.3	55.6	11.1	0.0
2%Al_2O_3	32.7	54.4	10.9	2.0
5%Al_2O_3	31.7	52.9	10.6	4.8
8%Al_2O_3	30.9	51.4	10.3	7.4
9%Al_2O_3	30.6	51.0	10.2	8.2
10%Al_2O_3	30.3	50.5	10.1	9.1

2.2. Characterization

X-ray diffraction (Bruker D8 Advance diffractometer with CuKα radiation ($\lambda_{K\alpha}$ = 0.15406 nm)) was performed on ground powders to identify the crystalline phases. Diffractograms were recorded between 15° and 80° with steps of 0.021° for a total acquisition time of 2 h.

After being embedded in epoxy resin, the samples were mirror polished. The cross sections were observed by using a Scanning Electron Microscope JEOL JSM-6010 LA (voltage = 15 kV, working distance = 10 mm).

The compositions of the precipitated phases and of the glassy matrix were determined through Electron Probe MicroAnalysis (EPMA) measurements performed on a JEOL JXA-8530F. The conditions used for the analyses were an acceleration voltage of 15 kV and a beam intensity of 20 nA. The standards used were wollastonite $CaSiO_3$ for Ca, albite $NaAlSi_3O_8$ for Al and Si, and yttrium disilicate $Y_2Si_2O_7$ for Y. Oxygen concentration was calculated by stoichiometry assuming that the valences states of cations are 2, 3, 4 and 3 for Ca, Al, Si and Y respectively.

The results of the quantifications are averaged from 10 measurements and the error bars correspond to standard deviation.

3. Results and discussions

3.1. Influence of alumina addition in the $C_{22}S_{70}Y_8$ system

The heat treated $C_{22}S_{70}Y_8$ samples added with alumina exhibit a spread in the $Pt_{95}Au_5$ crucibles that increases with the alumina content. This simple observation suggests a liquid proportion increasing with the addition of alumina to the mix.

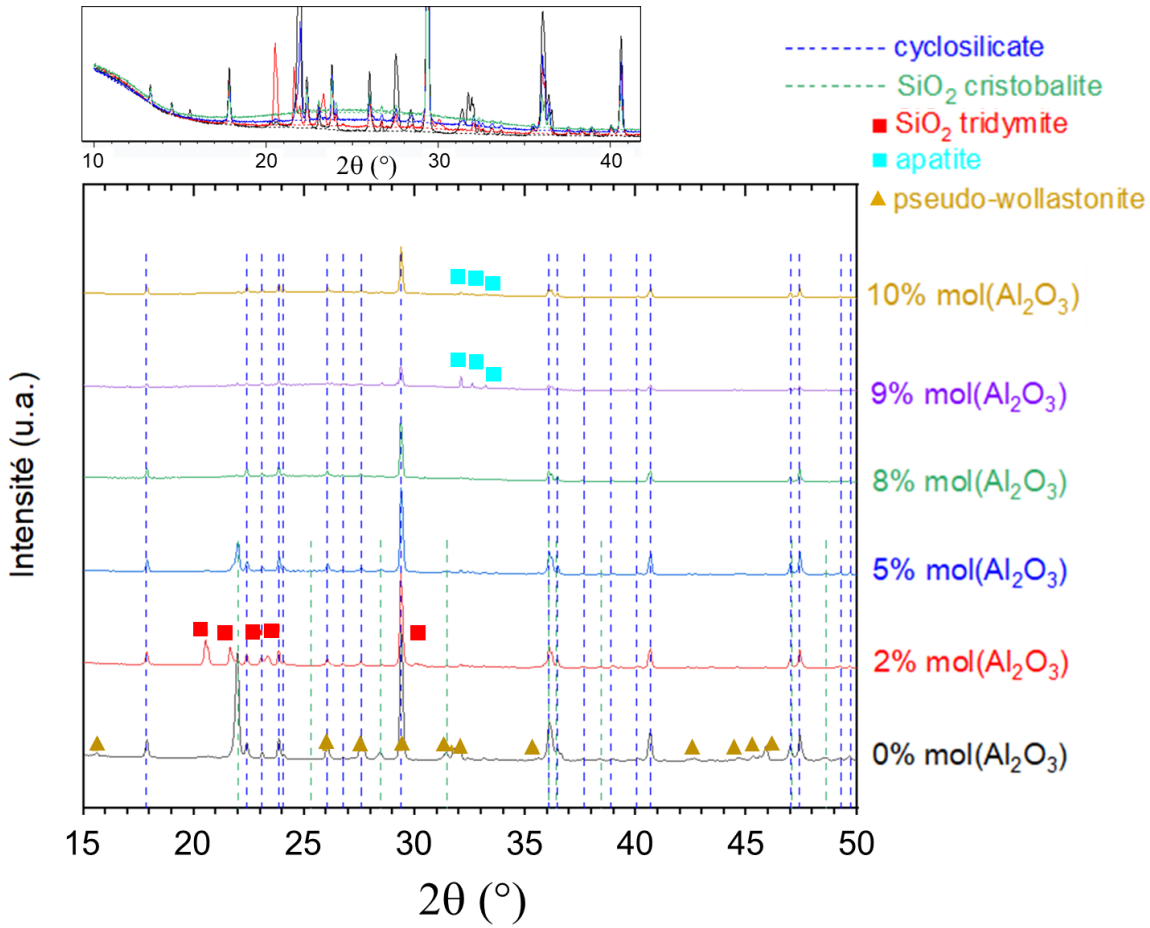

Figure 2. X-ray diffraction pattern of $C_{22}S_{70}Y_8$ with addition of alumina from 0 to 10 mol.% after heat treatment at 1300°C for 260 hours. The diffractograms in the insert correspond to the samples with alumina addition from 0 to 8 mol.% without subtraction of the background.

All the diffractograms of the heat treated samples presented in Figure 2 show exhibit the presence of rare-earth-rich crystalline phases such as apatite [16], cyclosilicate [17] and other

phases as pseudo-wollastonite [18] and silica [19,20]. The intensity of the bump at angles in the 20°-35° range increasing with the alumina content (insert in Figure 2) confirms the higher proportion of liquid phase. Pseudo-wollastonite $CaSiO_3$ is only detected in the sample with no alumina addition (see peak at $2\theta = 31.9°$). Tridymite and cristobalite allotropic forms of silica SiO_2 are detected for the low amounts of added alumina (0 to 2 mol.%). Yttrium cyclosilicate $Ca_3Y_2Si_6O_{18}$ (main peak of the phase at $2\theta = 29.4°$) appears in all the sample, and apatite $Ca_2Y_8(SiO_4)_6O_2$ is only identified with the highest added alumina contents (9 and 10 mol.%). Crystallized phase containing alumina are never detected, which suggests that alumina is totally contained in the liquid phase.

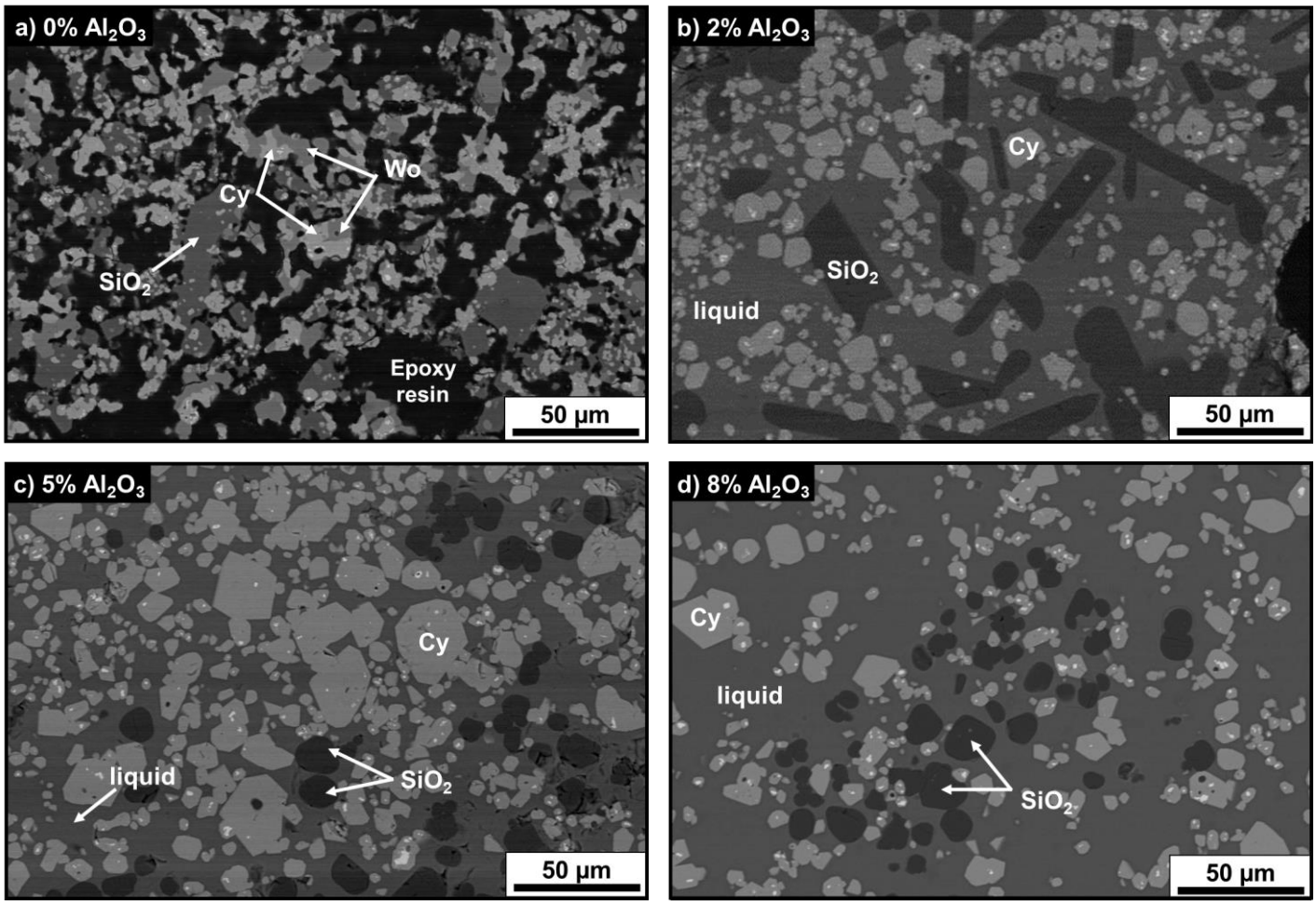

Figure 3. SEM micrographs (Back Scattered Electrons mode) of $C_{22}S_{70}Y_8$ samples without addition of alumina (a), and with addition of 2 mol.% (b), 5 mol.% (c) and 8 mol.% (d) of alumina after heat treatment at 1300°C for 260 hours.

Micrographs (Back Scattered Electrons – BSE – mode) of the samples added with up to 8 mol.% are presented in Figure 3. Three contrasts can be observed in the alumina-free sample (Figure 3a). The clearest phase is identified as the rare-earth-rich one, yttrium cyclosilicate $Ca_3Y_2Si_6O_{18}$

(Cy), which is consistent with the XRD pattern of Figure 2. The darkest phase is silica SiO_2 (in its cristobalite form according to XRD), and the intermediate contrast phase is pseudo-wollastonite (Wo). The formation of a liquid phase in the $C_{22}S_{70}Y_8$ mix at 1300°C seems to not be possible without Al_2O_3, whereas it is observed at 1400°C by Poerschke et al. [9]. The extent of this liquid field is very narrow at 1400°C (Figure 1), so its absence at 1300°C can be considered, allowing in this case an equilibrium of silica and cyclosilicate with pseudo-wollastonite as observed on Figure 2 and 3a. It must be noted here that some clear spots can be observed in the cyclosilicate precipitates, revealing very small amounts of an yttrium rich phase: as this phase is never in contact with the liquid, it will not be taken into account in the equilibria described here and further.

A liquid phase can be observed (with an intermediate grey contrast in BSE mode) when at least 2 mol.% of alumina is added to the mix (Figure 3b-d). In these cases, the liquid phase is in equilibrium with cyclosilicate and silica, which is still confirmed by XRD analyses (Figure 2). Silica is present as allotropic form of cristobalite when Al_2O_3 content is equal to 0 and 5 mol.%, and as tridymite when Al_2O_3 content is equal to 2 mol.%. Silica transition from cristobalite to tridymite is supposed to occur at 1470°C, but previous work by Araori et al. have shown that in presence of Al_2O_3 a lower transition temperature can be observed [21]. However, this is does not explain the presence of the cristobalite form of SiO_2 when alumina is not present in the mix. In all cases of Figure 3 the homogeneous BSE contrast of cyclosilicate demonstrates the homogeneity of the composition of this phase.

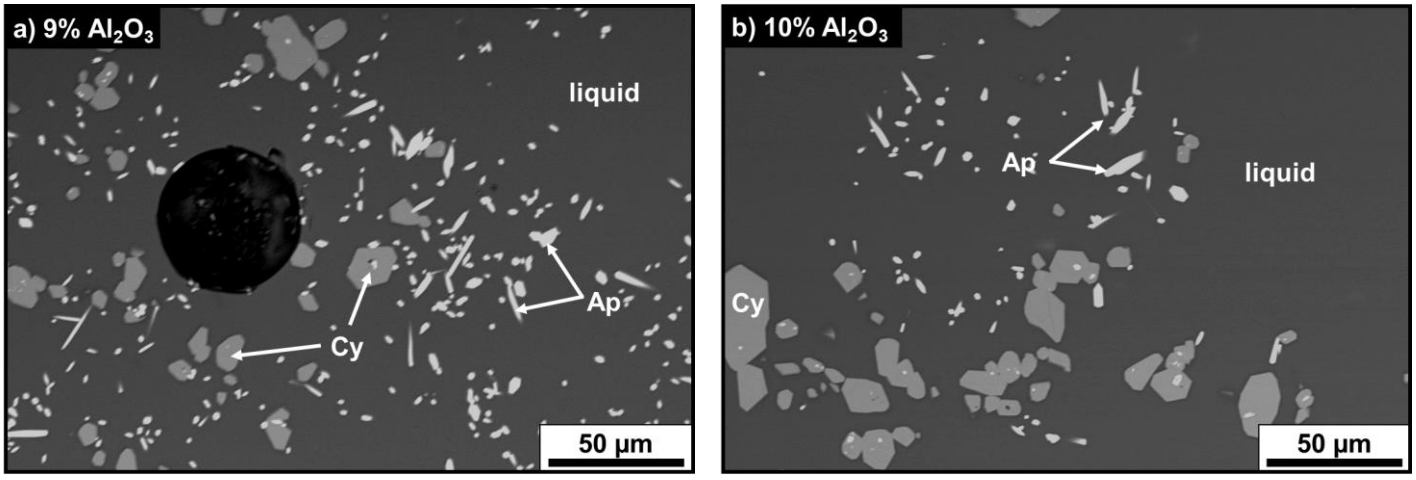

Figure 4. SEM micrographs (Back Scattered Electrons mode) of $C_{22}S_{70}Y_8$ samples with addition of 9 mol.% (a) and 10 mol.% (b) of alumina after heat treatment at 1300°C for 260 hours.

Micrographs of samples with higher alumina (addition of 9 and 10 mol.%) contents are presented on Figure 4. In addition to cyclosilicate, apatite phase $Ca_2Y_8(SiO_4)_6O_2$ is identified in both cases, confirmed by XRD patterns of Figure 2. Apatite exhibits a needle-like morphology, and its high yttrium content explains its very clear contrast in BSE mode. A large amount of liquid phase is also observed in these samples. Homogeneous composition of the crystallized apatite phase is confirmed by EPMA measurements, for all alumina contents, with a value of Ca/Si ratio around 0.34±0.01 (theoretical ratio in stoichiometric apatite Ca/Si = 0.33). This homogeneous stoichiometric composition is observed despite the large solid solution observed for apatite on the ternary $CaO\text{-}SiO_2\text{-}YO_{1.5}$ phase diagram [9]

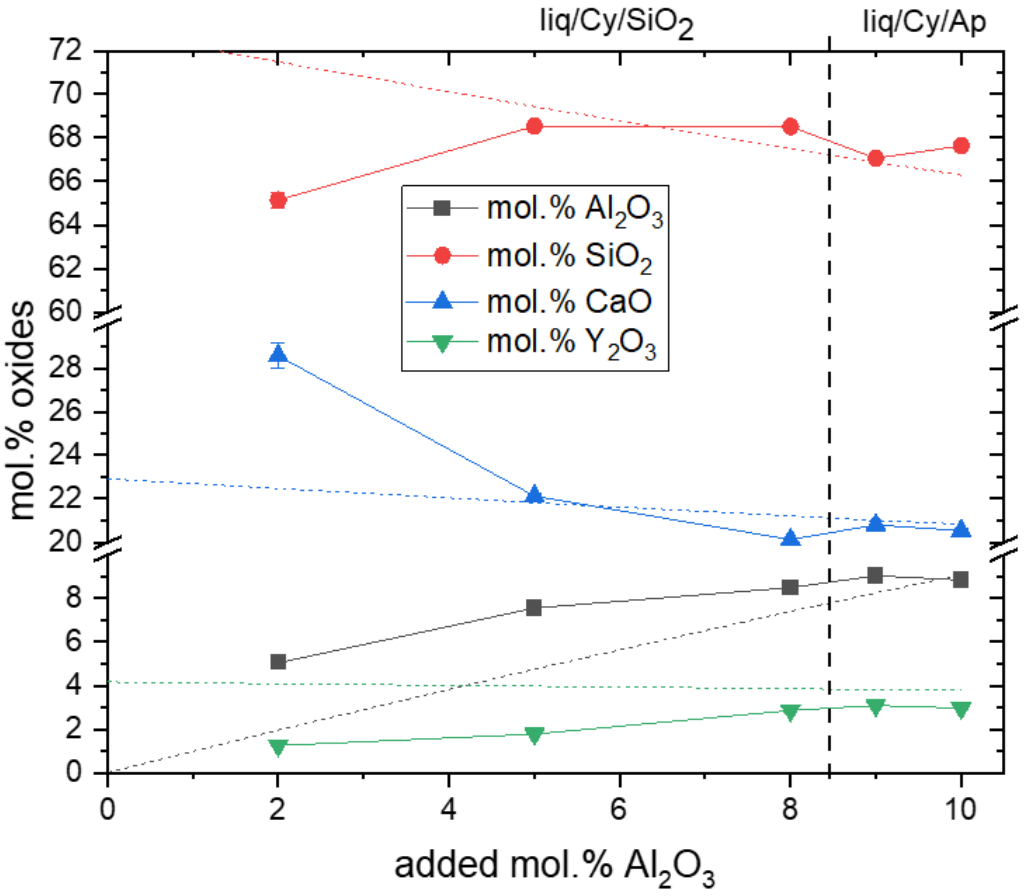

Figure 5. Evolution of the liquid composition as a function of the alumina added to $C_{22}S_{70}Y_8$ after heat treatment at 1300°C for 260 hours. The dotted lines represent the evolution of the composition of the initial mixes.

The evolution of the liquid composition with alumina content (starting from an addition of 2 mol.% of alumina) is reported in Figure 5 thanks to EPMA measurements. The dotted lines represent the evolution of the initial mix composition (before heat treatment). It can be noticed

that an increasing addition of alumina leads alumina, calcia and silica content in the liquid which are getting close to their respective values in the initial mix. This shows that the proportion of liquid increases with the addition of alumina. The silica (acidic oxide) content is increasing and the calcia content (basic oxide) is decreasing: the acidity of the liquid is thus increasing with the alumina content. When apatite phase starts to precipitate, Al_2O_3, CaO and Y_2O_3 contents become constant, despite the increasing addition of alumina. The yttrium content increases with the addition of alumina to the mix. As Y_2O_3 can be considered as a basic oxide, the acidification of the mix due to the addition of alumina can explain the increasing solubility of yttrium, as previously observed by Perrudin et al. [22]. Then yttrium content remains constant around 2 at.% when the apatite phase precipitates.

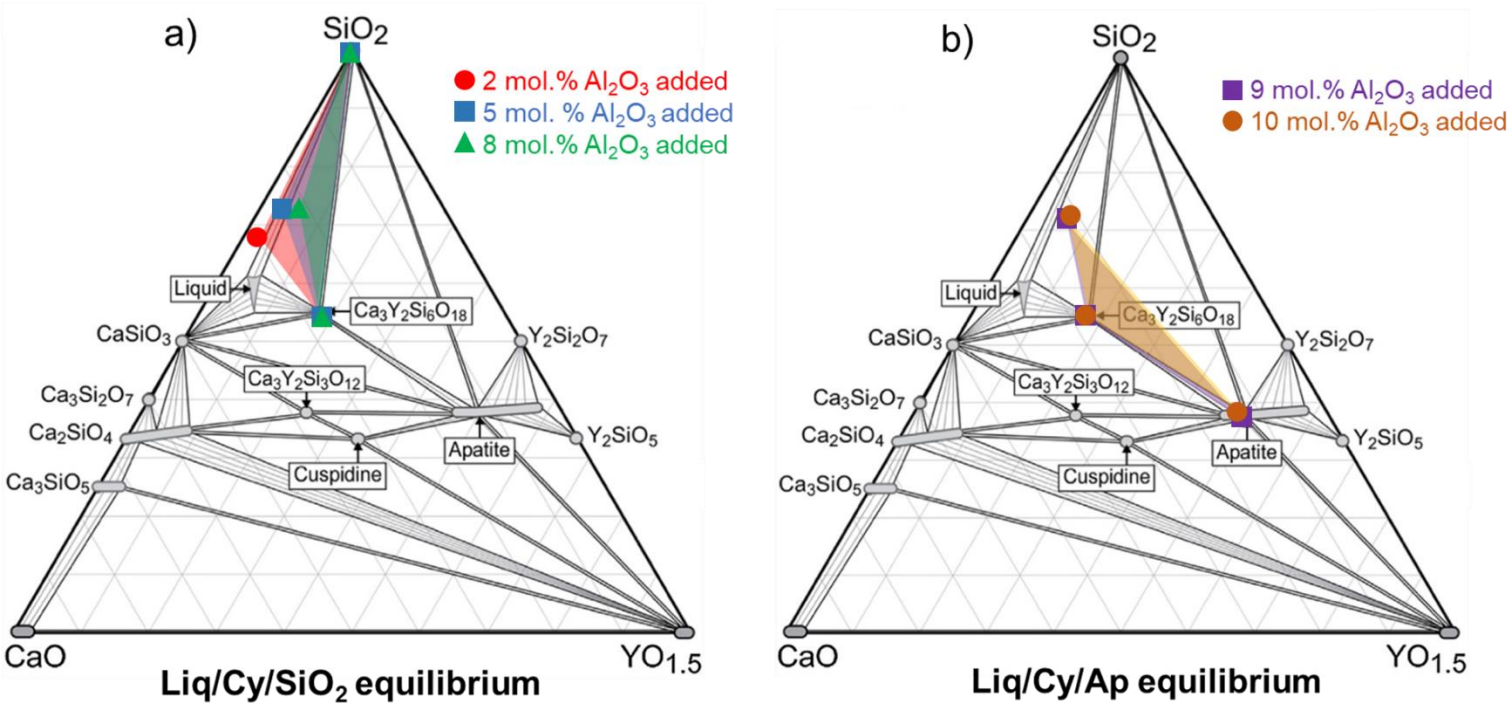

Figure 6. Influence of the addition of 2 to 8 mol.% of Al_2O_3 (a) and of 9 to 10 mol.% of Al_2O_3 (b) on the equilibria observed in the CaO-SiO_2-$YO_{1.5}$ for the $C_{22}S_{70}Y_8$ at 1300°C, and reported in the phase diagram proposed by Poerschke et al. at 1400°C [9].

The identification of the phases and the evolution of the melt composition highlight the influence of alumina addition in the CaO-SiO_2-Y_2O_3 system. The identified equilibria after heat treatment at 1300°C are reported in Figure 6, based on the ternary diagram provided by Poerschke et al. [9] for the same system at 1400°C. Figure 6a describes the equilibria observed for alumina additions rising from 2 to 8 mol.%. In this case, addition of alumina leads to an extent of the liquid field towards a more acidic, silica-rich medium, resulting in a higher dissolution of the basic yttrium oxide Y_2O_3. Figure 6b shows that for 9 and 10 mol.% of added

alumina the equilibrium state is not the same, despite a liquid composition close to the one measured for 8 mol.% of added alumina: in this case, the liquid is in equilibrium with cyclosilicate and apatite and its composition remains constant.

3.2. Influence of alumina addition in the $C_{30}S_{50}Y_{20}$ system

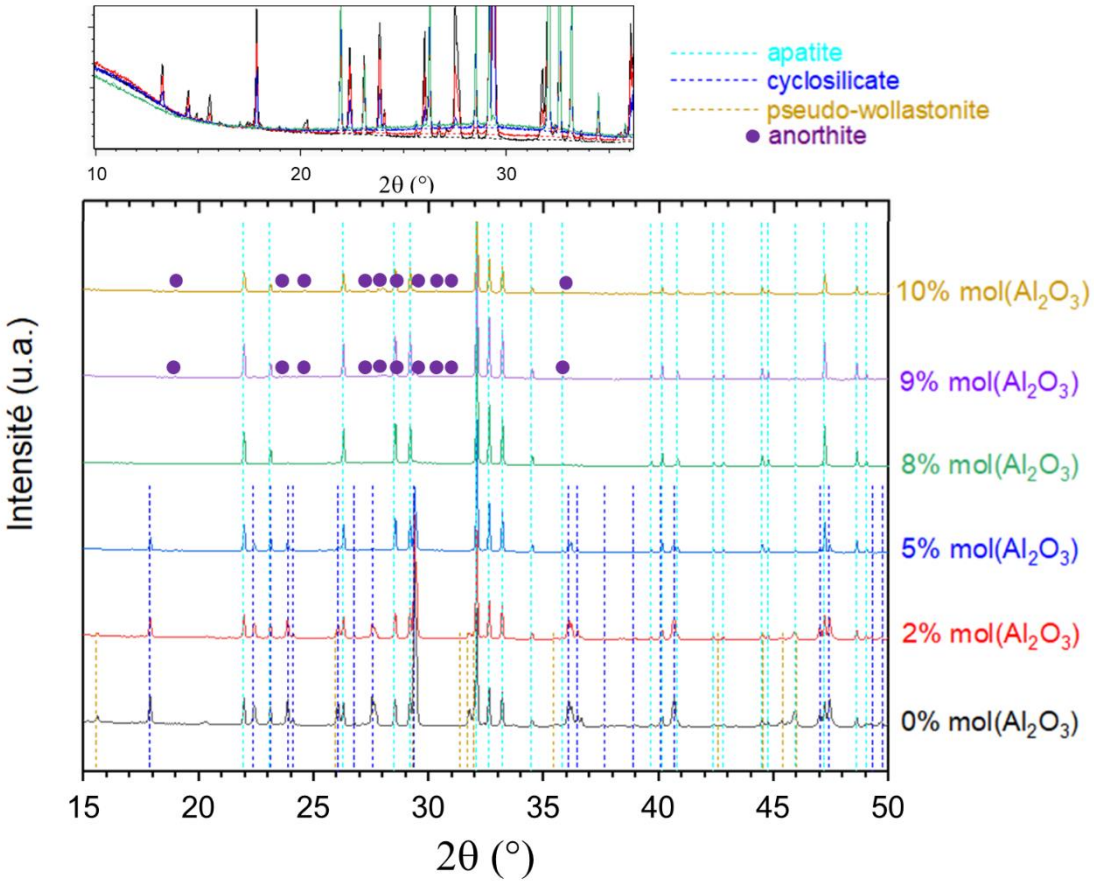

Figure 7. X-ray diffraction pattern of $C_{30}S_{50}Y_{20}$ with addition of alumina from 0 to 10 mol.% after heat treatment at 1300°C for 260 hours. The diffractograms in the insert correspond to the samples with alumina addition from 0 to 8 mol.% without subtraction of the background.

In the same way as for alumina doped $C_{22}S_{70}Y_8$ samples, the spread of the alumina doped $C_{30}S_{50}Y_{20}$ samples in the $Pt_{95}Au_5$ crucibles suggest a liquid proportion increasing with their alumina content. This is confirmed by the XRD analysis (insert in Figure 7) by the increase of the intensity of the bump in the 20°-35° angle range. Yttrium-rich precipitated phases as cyclosilicate and apatite are detected (Figure 7) : yttrium apatite appears for all alumina contents, and cyclosilicate is detected for the lower alumina contents (for additions up to 5 mol.% Al_2O_3). Other phases are observed, as pseudo-wollastonite [18] for low alumina contents (addition of 0

and 2 mol.% Al_2O_3), and anorthite $CaAl_2Si_2O_8$ (peak at $2\theta = 29.7°$) for the highest alumina contents (addition of 9 and 10 mol.% Al_2O_3) [23]. Contrary to the $C_{22}S_{70}Y_8$ series, silica is never detected here.

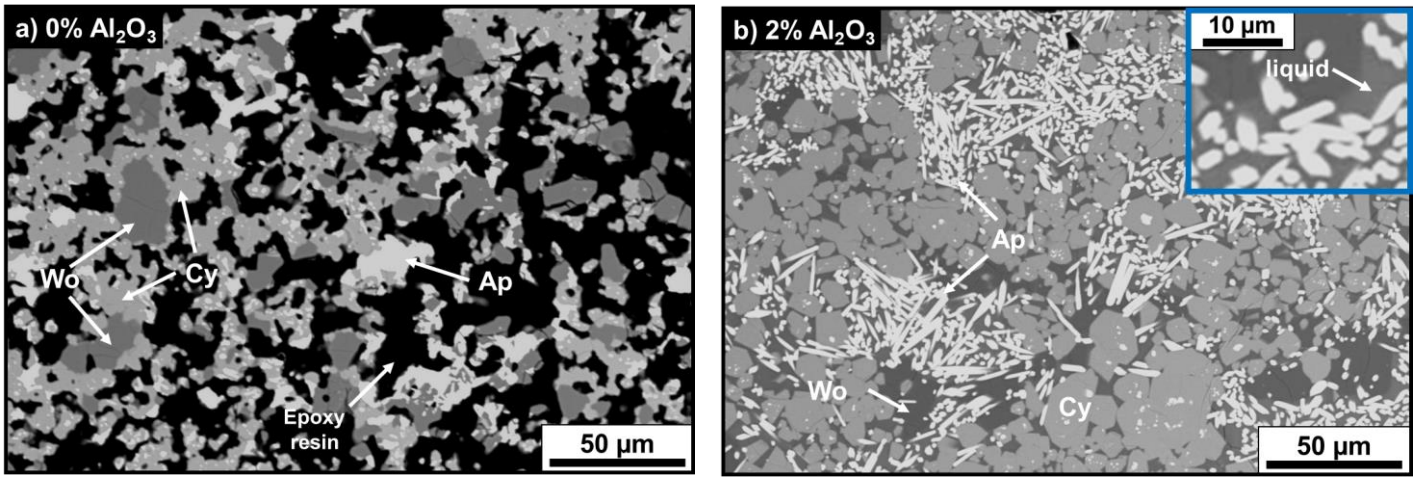

Figure 8. SEM micrographs (Back Scattered Electrons mode) of $C_{30}S_{50}Y_{20}$ samples without addition of alumina (a), and with addition of 2 mol.% (b) of alumina after heat treatment at 1300°C for 260 hours.

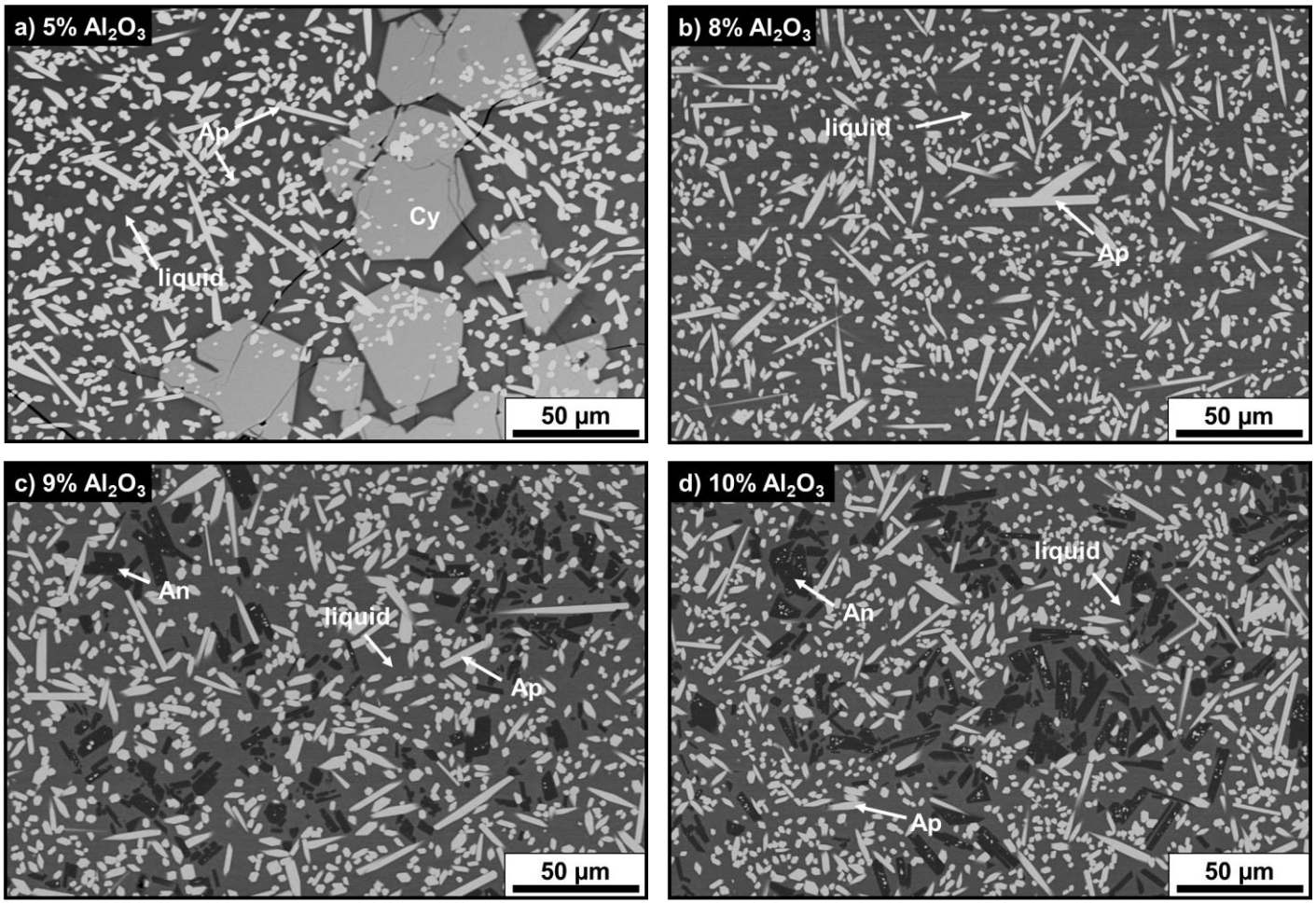

Figure 9. SEM micrographs (Back Scattered Electrons mode) of $C_{30}S_{50}Y_{20}$ samples with addition of 5 mol.% (a), 8 mol.% (b), 9 mol.% (c) and 8 mol.% (d) of alumina after heat treatment at 1300°C for 260 hours.

The presence of pseudo-wollastonite is confirmed by the micrograph of the sample 0 and 2 mol.% of added alumina (Figure 8), and yttrium-rich phases apatite and cyclosilicate appear a clearer chemical contrast. The addition of 2 mol.% of alumina generates the appearance of a little amount of liquid (insert in Figure 8b). The needle-like acicular morphology of apatite can be linked to the presence of this liquid during its precipitation. This kind of morphology is not observed when apatite precipitates in absence of a liquid phase, as previously observed by Panteix et al. [24]. The micrographs of samples added with 5, 8, 9 and 10 mol.% of alumina confirm the increase of the liquid phase proportion with alumina addition (Figure 9). For 5 mol.% of added alumina (Figure 9a), the liquid phase is in equilibrium with apatite and cyclosilicate. For the higher alumina contents (Figures 9b, c and d), cyclosilicate is not observed anymore. For 9 and 10 mol.% of added alumina, the presence of an alumina-rich phase, i.e. anorthite, is detected (Figures 9c and d). All these observations are in consistent with the XRD analysis of Figure 7.

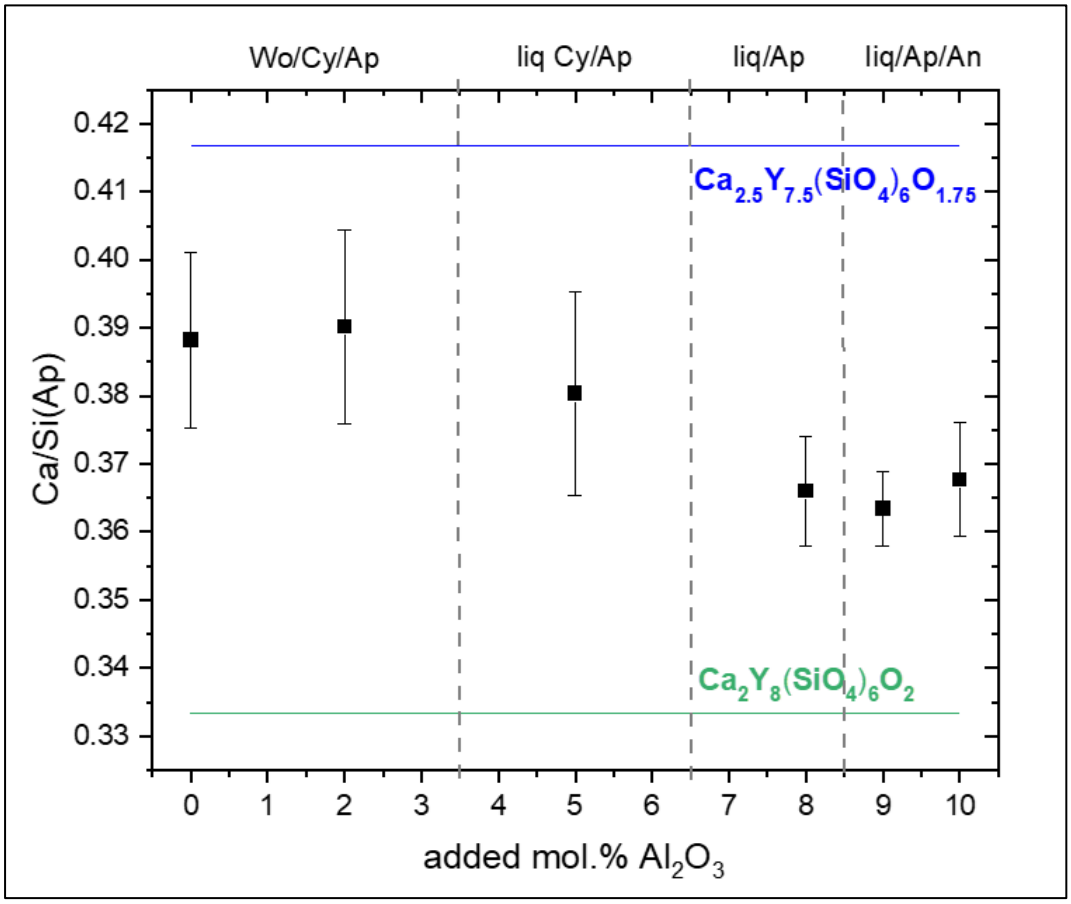

Figure 10. Evolution of the Ca/Si ratio of the precipitated apatite phase in $C_{30}S_{50}Y_{20}$ samples as a function of added alumina.

The evolution of the Ca/Si ratio in the apatite phase formed in the samples of the $C_{30}S_{50}Y_{20}$ series has been measured by EPMA and is reported in Figure 10. Contrary to the $C_{22}S_{70}Y_8$ series, the composition of the precipitated apatite phase does not correspond to the stoichiometric formulation $Ca_2Y_8(SiO_4)_6O_2$. For the lowest additions of alumina (0 and 2 mol.%), the Ca/Si ratio is constant, with the highest value, which is also the furthest from the defect free composition $Ca_2Y_8(SiO_4)_6O_2$. Starting from 5 mol.% of added alumina, the Ca/Si ratio then decreases. Considering the standard deviations of the measurements, it is impossible to propose an accurate formulation of the precipitated apatites. However, regardless the amount of added alumina, the Ca/Si ratio of all the apatites precipitated in this series does not correspond to the value of the defect free apatite $Ca_2Y_8(SiO_4)_6O_2$ (Ca/Si = 0.33) systematically observed in the $C_{22}S_{70}Y_8$ series. The first constant value (0, 2 and 5 mol.% of added alumina) is about 0.39, and the second value (more than 8 mol.% of added alumina) is about 0.37.

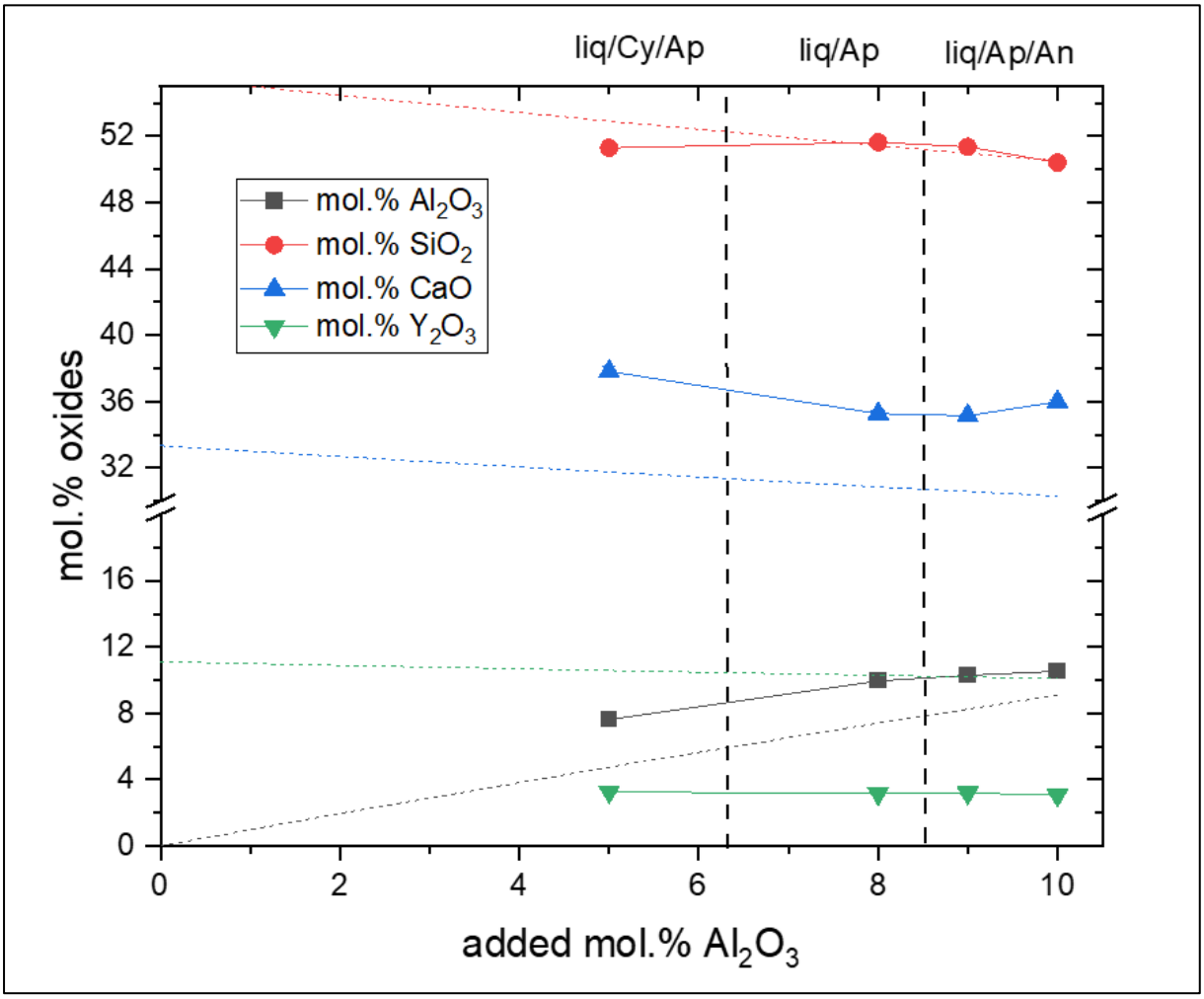

Figure 11. Evolution of the liquid composition as a function of the alumina added to $C_{30}S_{50}Y_{20}$ after heat treatment at 1300°C for 260 hours. The dotted lines represent the evolution of the composition of the initial mixes.

EPMA measurements of the evolution of the oxides proportions in the liquid with the addition of alumina are reported in Figure 11. Al_2O_3 content in the liquid is increasing whit alumina addition up to 8 mol.%, which is consistent with the fact that the liquid is the only phase containing alumina. For higher amounts of added alumina, the precipitation of the Al containing phase anorthite $CaAl_2Si_2O_8$ leads to a less important increase of the concentration of Al_2O_3 in the melt. The liquid composition stops to get close to the composition of the initial mix (dotted lines on Figure 11) when anorthite starts to precipitate (alumina addition of 9 and 10 mol.% Al_2O_3), thus showing that the proportion of liquid does not increase anymore. For the highest amounts of added alumina, it can be considered that the melt becomes more basic, as the proportion of SiO_2 decreases while the proportion of CaO increases. Y_2O_3 solubility is not significantly affected by the addition of alumina to the initial mix, and is about 2.2 at.% Y.

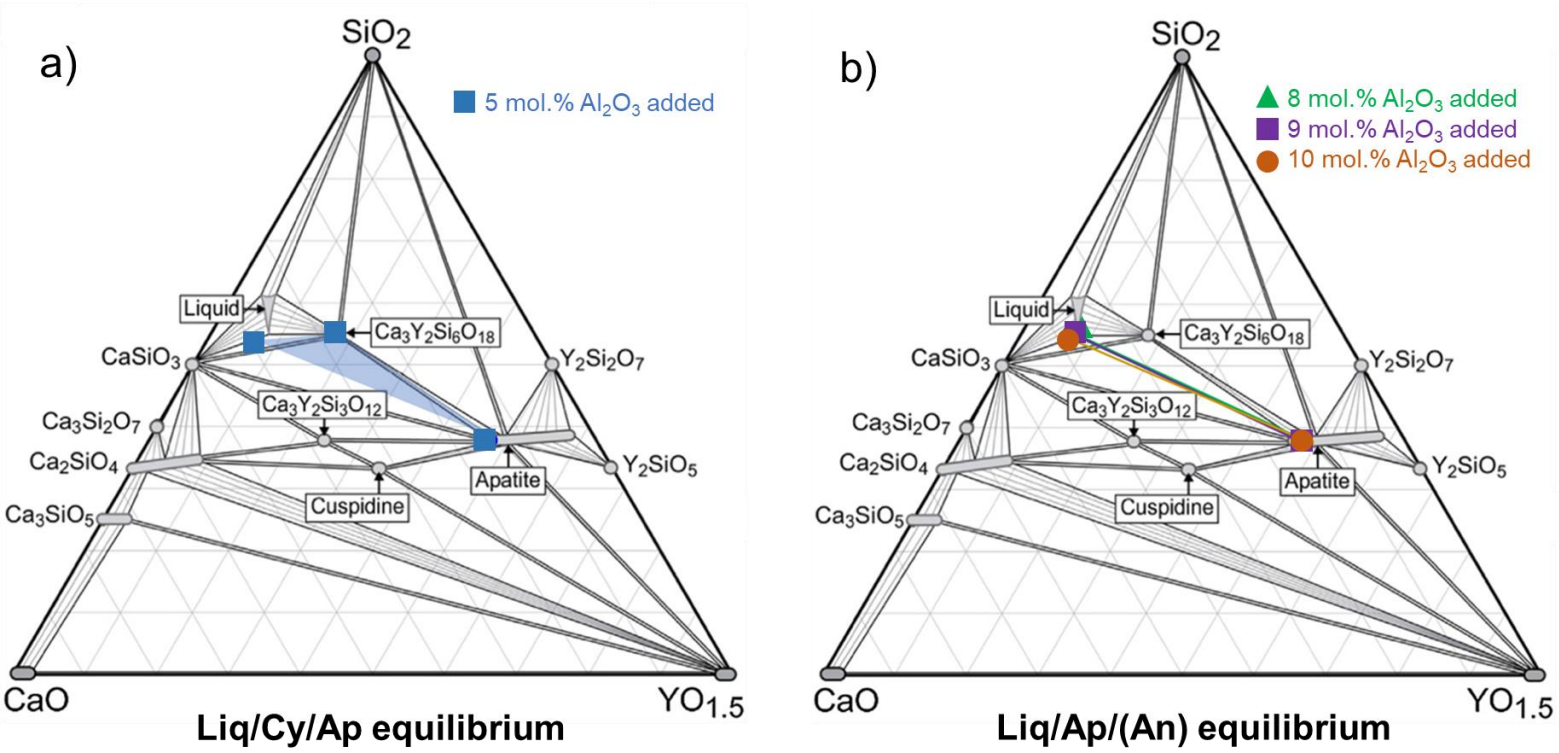

Figure 12. Influence of the addition of 5 mol.% of Al_2O_3 (a) and of 8 to 10 mol.% of Al_2O_3 (b) on the equilibria observed in the CaO-SiO_2-$YO_{1.5}$ for the $C_{30}S_{50}Y_{20}$ at 1300°C, and reported in the phase diagram proposed by Poerschke et al. at 1400°C [9].

Concerning the equilibrium state in the $C_{30}S_{50}Y_{20}$, the system without alumina is a three-phased equilibrium between apatite, cyclosilicate and pseudo-wollastonite. This is consistent with the isotherm section of the ternary phase diagram proposed by Poerschke et al. in the CaO-SiO_2-Y_2O_3 system at 1400°C [9]. The three-phased equilibrium between liquid, cyclosilicate and apatite, observed when 5 mol.% alumina is added is represented in Figure 12a. For 8, 9 and 10

mol.% of added alumina, the equilibria between apatite and the liquids are represented in Figure 12b. The equilibria represented in Figure 12 emphasize that the addition of alumina in the $C_{30}S_{50}Y_{20}$ system has a very low impact on the liquid composition, which remains close to one predicted by the phase diagram and corresponds to the silica-poor composition. It can be concluded that in this system, the addition of alumina has no impact on the extent of the liquid field and leads to a modification of the equilibria.

3.3. Influence of alumina on the liquid field of $CaO\text{-}SiO_2\text{-}YO_{1.5}$ system

From all the previous experimental results; it is possible to have an accurate representation of the extent of the liquid field for a given system at 1300°C.

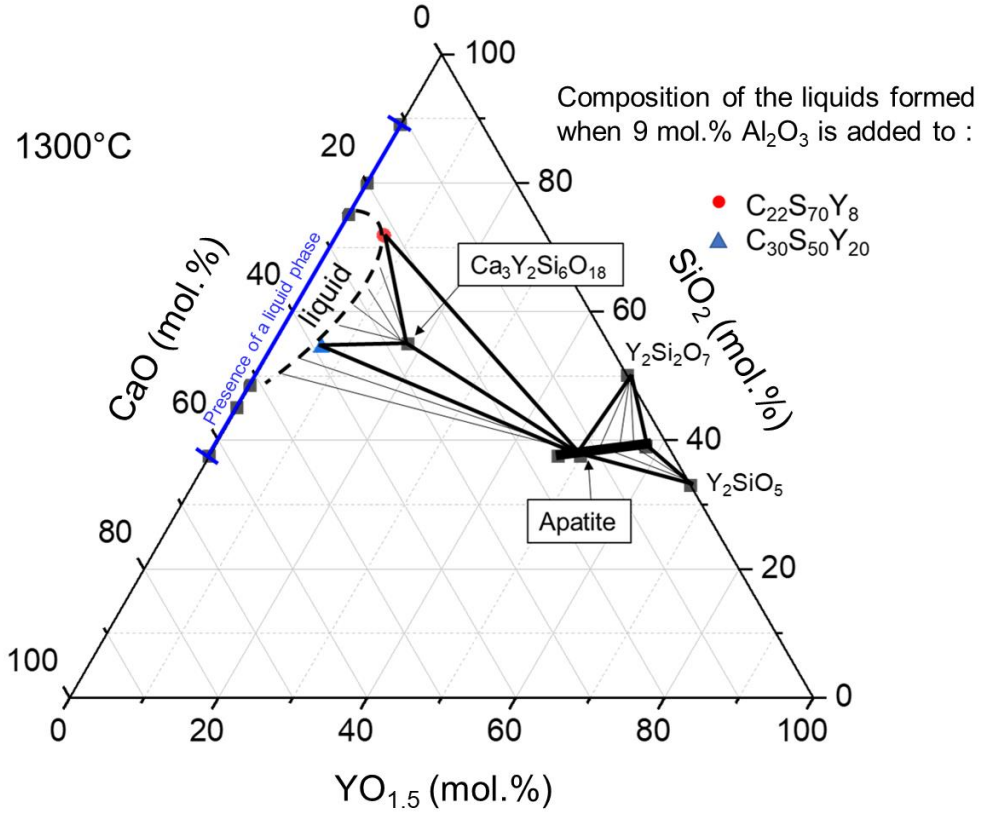

Figure 13. Modified isothermal section of the ternary $CaO\text{-}SiO_2\text{-}YO_{1.5}$ system at 1300°C in presence of addition of 9 mol.% of Al_2O_3.

Figure 13 represents the modified isothermal section of the ternary $CaO\text{-}SiO_2\text{-}YO_{1.5}$ system at 1300°C in presence of addition of 9 mol.% of alumina. The blue lines represents the region of the $CaO\text{-}SiO_2\text{-}Al_2O_3$ system, calculated thanks to FactSage [25] for 9 mol.% of alumina, where a liquid is present. The EPMA measurements of the liquid compositions in the two $C_{22}S_{70}Y_8$

and $C_{30}S_{50}Y_{20}$ systems at equilibrium are also reported in Figure 13. The dotted black line represents an assumed limit of the liquid field in the $CaO\text{-}SiO_2\text{-}YO_{1.5}$ system at 1300°C with an addition of 9 mol.% of alumina. This limit includes the eutectic compositions of the $CaO\text{-}Al_2O_3\text{-}SiO_2$ system at 1300°C [25], and the two compositions of the liquids measured by EPMA.

4. Conclusions

The study of the two $C_{22}S_{70}Y_8$ and $C_{30}S_{50}Y_{20}$ systems added with 2 to 10 mol.% Al_2O_3 has given access to supplementary thermodynamic data in the $CaO\text{-}AlO_{1.5}\text{-}SiO_2\text{-}YO_{1.5}$ quaternary system at 1300°C.

In absence of alumina addition, the acidic system $C_{22}S_{70}Y_8$ does not exhibit any liquid phase at 1300°C. Starting from 2 mol.% of added alumina, a liquid field appears in equilibrium with silica and cyclosilicate. The composition of this liquid becomes more and more acidic as the addition of alumina increases up to 8 mol.%, leading to an increasing solubility limit of the basic oxide Y_2O_3 in the melt. The largest additions of alumina (9 and 10 mol.%) lead to the precipitation of an homogeneous apatite phase (close to the stoichiometric $Ca_2Y_8(SiO_4)_6O_2$ composition) in equilibrium with the liquid and cyclosilicate. For both alumina contents, the liquid composition and the solubility of Y_2O_3 remain constant.

As expected, the alumina free $C_{30}S_{50}Y_{20}$ basic system exhibits an equilibrium between pseudo-wollastonite, apatite and cyclosilicate at 1300°C. The small addition of alumina (2 mol.%) generates a little amount of liquid. Then the largest alumina additions lead to the disappearance of cyclosilicate and to the establishment of an equilibrium between a liquid of constant composition (with a constant solubility of Y_2O_3) and an apatite phase with a Ca/Si ratio slightly decreasing with the addition of alumina.

The liquid field of the $CaO\text{-}SiO_2\text{-}Al_2O_3$ system for a given alumina content and the liquid compositions determined experimentally can then be incorporated in the ternary phase diagram $CaO\text{-}SiO_2\text{-}YO_{1.5}$ at 1300°C. It is then possible to have an accurate representation of the extent of the liquid field for a given alumina content. Consequently, the existing equilibria can be identified, giving access to the relative stabilities of phases as apatite and cyclosilicates in these systems.

References

[1] D. LaChapelle, M. Noe, W. Edmondson, H. Stegemiller, J. Steibel, D. Chang, CMC materials applications to gas turbine hot section components, in: 34th AIAA/ASME/SAE/ASEE Joint Propulsion Conference and Exhibit. American Institute of Aeronautics and Astronautics, Cleveland, Ohio, USA (1998). https://doi.org/10.2514/6.1998-3266

[2] K.N. Lee, D.S. Fox, N.P. Bansal, Rare earth silicate environmental barrier coatings for SiC/SiC composites and Si_3N_4 ceramics, J. Eur. Ceram. Soc. 25 (2005) 1705–1715. https://doi.org/10.1016/j.jeurceramsoc.2004.12.013

[3] K.M. Grant, S. Krämer, J.P.A. Löfvander, C.G. Levi, CMAS degradation of environmental barrier coatings, Surf. Coat. Tech. 202 (2007) 653–657. https://doi.org/10.1016/j.surfcoat.2007.06.045

[4] K.M. Grant, S Krämer, G.G.E. Seward, C.G. Levi, Calcium–Magnesium Alumino-Silicate interaction with yttrium monosilicate Environmental Barrier Coatings, J. Am. Ceram. Soc. 93 (2010) 3504–3511. https://doi.org/10.1111/j.1551-2916.2010.03916.x

[5] S. Krämer, J. Yang, C.G. Levi, Infiltration-inhibiting reaction of gadolinium zirconate Thermal Barrier Coatings with CMAS melts, J. Am. Ceram. Soc. 91 (2008) 576–583. https://doi.org/10.1111/j.1551-2916.2007.02175.x

[6] J. Liu, L. Zhang, Q. Liu, L. Cheng, Y. Wang, Calcium–magnesium–aluminosilicate corrosion behaviors of rare-earth disilicates at 1400°C, J. Eur. Ceram. Soc. 33 (2013) 3419–3428. https://doi.org/10.1016/j.jeurceramsoc.2013.05.030

[7] D.L. Poerschke, J.H. Shaw, N. Verma, F.W. Zok, C.G. Levi, Interaction of yttrium disilicate environmental barrier coatings with calcium-magnesium-iron alumino-silicate melts. Acta. Mater. 145 (2018) 451–461. https://doi.org/10.1016/j.actamat.2017.12.004

[8] W.D. Summers, D.L. Poerschke, D. Park, J.H. Shaw, F.W. Zok, C.G. Levi, Roles of composition and temperature in silicate deposit-induced recession of yttrium disilicate, Acta. Mater. 160 (2018) 34-46. https://doi.org/10.1016/j.actamat.2018.08.043

[9] D.L. Poerschke, T.L. Barth, O. Fabrichnaya, C.G. Levi, Phase equilibria and crystal chemistry in the calcia–silica–yttria system, J. Eur. Ceram. Soc. 36 (2016) 1743–1754. https://doi.org/10.1016/j.jeurceramsoc.2016.01.046

[10] D.L. Poerschke, C.G. Levi, Phase equilibria in the calcia-gadolinia-silica system, J. Alloys Compd. 695 (2017) 1397–1404. https://doi.org/10.1016/j.jallcom.2016.10.263

[11] N.P. Bansal, S.R. Choi, Properties of CMAS glass from desert sand, Ceram. Int. 41 (2015) 3901–3909. https://doi.org/10.1016/j.ceramint.2014.11.072

[12] U. Kueppers, C. Cimarelli, K.U. Hess, J. Taddeucci, F.B. Wadsworth, D.B. Dingwell, The thermal stability of Eyjafjallajökull ash versus turbine ingestion test sands, J. Appl. Volcanol. 3:4 (2014). https://doi.org/10.1186/2191-5040-3-4

[13] J.L. Smialek, The chemistry of Saudi arabian sand: a deposition problem on helicopter turbine airfoils, in Gordon Conference on Corrosion, New London, New Hampshire USA (1991).

[14] R.I. Webster, N.P. Bansal, J.A. Salem, E.J. Opila, V.L. Wiesner, Characterization of Thermochemical and Thermomechanical Properties of Eyjafjallajökull Volcanic Ash Glass. Coatings 10 (2020) 100. https://doi.org/10.3390/coatings10020100

[15] D.L. Poerschke, T.L. Barth, C.G. Levi, Equilibrium relationshsips between thermal barrier oxides and silicate melts, Acta Mater. 120 (2013) 302-314. http://dx.doi.org/10.1016/j.actamat.2016.08.077

[16] W.L. Wanmaker, J.W. ter Vrugt, J.G. Verlijsdonk, Luminescence of alkaline earth yttrium and lanthanum phosphate-silicates with apatite structure, J. Solid State Chem. 3 (1971) 452–457. https://doi.org/10.1016/0022-4596(71)90084-3

[17] H. Yamane, T. Nagasawa, M. Shimada, T. Endo, $Ca_3Y_2(Si_3O_9)_2$. Acta Crystallogr. Sect. C 53 (1997) 1533–1536. https://doi.org/10.1107/S010827019700721X

[18] T. Yamanaka, H. Mori, The structure and polytypes of α-$CaSiO_3$ (pseudowollastonite), Acta Crystallogr. Sect. B 37 (1981) 1010–1017. https://doi.org/10.1107/S0567740881004962

[19] H. Graetsch, I. Topalovlć-Dierdorf, I., 29Si MAS NMR spectrum and superstructure of modulated tridymite L3-To(MX-1), Eur. J. Mineral. 8 (1996) 103–114. https://doi.org/10.1127/ejm/8/1/0103

[20] D. Peacor, High-Temperature Single Crystal Study of Cristobalite Inversion, Z. Kristallogr. Cryst. Mater. 138 (1973) 274–298. https://doi.org/10.1524/zkri.1973.138.138.274

[21] T. Arahori, T. Suzuki, Transformation of tridymite to cristobalite below 1470° C in silica refractories, J. Mater. Sci. 22 (1987) 2248–2252. https://doi.org/10.1007/BF01132967

[22] F. Perrudin, M.H. Vidal-Setif, C. Rio, C. Petitjean, P.J. Panteix, M. Vilasi, Influence of rare earth oxides on kinetics and reaction mechanisms in CMAS silicate melts, J. Eur. Ceram. Soc 39 (2019) 4223-4232. https://doi.org/10.1016/j.jeurceramsoc.2019.06.036

[23] R.J. Angel, M.A. Carpenter, L.W. Finger, Structural variation associated with compositional variation and order-disorder behavior in anorthite-rich feldspars, Am. Mineral. 75 (1990) 150–162.

[24] P.J. Panteix, I. Julien, P. Abélard, D. Bernache-Assollant, Influence of porosity on the electrical properties of $La_{9.33}(SiO_4)6O_2$ oxyapatite, Ceram. Int. 34 (2008) 1579-1586. https://doi.org/10.1016/j.ceramint.2007.05.004

[25] C.W. Bale, E. Bélisle, P. Chartrand, S.A. Decterov, G. Eriksson, A.E. Gheribi, K. Hack, I.H. Jung, Y.B. Kang, J. Melançon, A.D. Pelton, S. Petersen, C. Robelin, J. Sangster, P. Spencer, M-A. Van Ende, FactSage thermochemical software and databases, 2010–2016, Calphad, 54 (2016) 35-53. http://dx.doi.org/10.1016/j.calphad.2016.05.002